Supplementary Information

Reconfigurable large-scale optoelectronic reservoir computing on programmable silicon photonic processor

Dengfei Tang[1,3], Fangchen Hu[5], Shiyue Hua[4], Shanshan Yu[4], Zhiteng Luo[1,2], Zhanhong Zhou[1,2] Junwen Zhang[1,2], Jianyang Shi[1,2], Wei Chu[5], Haiwen Cai[5], Nan Chi[1,2,*], Haibin Zhao[1,3*], Ziwei Li[1,2,*]

*Correspondence should be addressed to C.N. (nanchi@fudan.edu.cn), H.Z. (hbzhao@fudan.edu.cn) and Z.L. (lizw@fudan.edu.cn)

This Supplementary file includes:

Supplementary Notes 1-5

Supplementary Figures 1-6

Supplementary Tables l

Supplementary References

Supplementary Note 1: definition of reconfigurable topology structure

We opt for the topology derived from the delay-based scheme as baseline. For TD-RC, each input $\boldsymbol{u}(t)$ undergoes a sample-and-hold procedure, the held time constant T' is taken to be less than the period T of the delay, θ is considered as node duration and defined by $\theta = \frac{T'-T}{q}$, where $1 \leq q < N$, which introduces a coupling from each internal virtual node to the neighboring one[1]. The updates equation for each node state in the delay-based reservoir can be recursively computed at time step k and generalized as follows:

$$x_{i,k} = \begin{cases} \mathrm{e}^{-i\theta}\, x_{n,k-1} + \sum_{j=q}^{i}\left(1-\mathrm{e}^{-\theta}\right)e^{-(i-j)\theta} f\left(x_{j-1,k-1}, \mathbf{W}_{\mathrm{in},j}\, u_k\right)\ i < q < N \\ \mathrm{e}^{-i\theta}\, x_{n,k-1} + \sum_{j=1}^{i}\left(1-\mathrm{e}^{-\theta}\right)e^{-(i-j)\theta} f\left(x_{n-q+i,k-2}, \mathbf{W}_{\mathrm{in},i}\, u_k\right)\ 0 < i \leq q \end{cases} \tag{1}$$

The coefficients $\mathrm{e}^{-i\theta}$ correspond to the values found in the last column of equivalent interconnection matrix, while its diagonal and off-diagonal elements are given by $\left(1-\mathrm{e}^{-\theta}\right)\mathrm{e}^{-(i-j)\theta}$. These two components explicitly describe the state coupling between consecutive time steps and form the approximate interconnection matrix $\mathbf{W}_{\mathrm{FixedF}} \in \mathbb{R}^{N\times N}$:

$$\mathbf{W}_{\mathrm{FixedF}}(i,j) = \begin{cases} \left(1-\mathrm{e}^{-\theta}\right)\mathrm{e}^{-(i-j)\theta},\ \text{if } j \leq \mathrm{N}-1 \\ \mathrm{e}^{-i\theta}, \text{if } j = \mathrm{N} \end{cases} \tag{2}$$

For reconfigured topology $\mathbf{W}_{\mathrm{RandF}} \in \mathbb{R}^{N\times N}$, shares the same structure as $\mathbf{W}_{\mathrm{FixedF}}$. Differently, the values of each diagonal and lower sub-diagonal are randomly generated. We have defined the mathematical expression for this structure as:

$$\mathbf{W}_{\mathrm{RandF}} = (1-R) * \mathbf{W}_{\mathrm{FixedF}} + (R * \mathbf{W}_{\mathrm{FixedF}}) * \mathrm{rand}(0,1) \tag{3}$$

$R \in [0,1]$ reflects the randomness of the values of the lower sub-diagonal elements. The higher the R value, the more random the coupling of node states. When randomness parameter R is set to 0, topology $\mathbf{W}_{\mathrm{RandF}}$ transforms into $\mathbf{W}_{\mathrm{FixedF}}$.

$\mathbf{W}_{\mathrm{RandF}}$ allows current node states to be coupled to the forward nodes with adjustable connection weights. By rotating $\mathbf{W}_{\mathrm{RandF}}$ counterclockwise by 180 degrees, coupling to backward nodes is achieved. Combining these two connection modes results in the bidirectional coupling topology $\mathbf{W}_{\mathrm{RandFB}} \in \mathbb{R}^{N\times N}$:

$$\mathbf{W}_{\mathrm{RandFB}} = \mathbf{W}_{\mathrm{RandF}} + \mathrm{rot180}(\mathbf{W}_{\mathrm{RandF}}) \tag{4}$$

The variations of the topology structures with changes in node duration θ and randomness R are presented in Supplementary Figures 1 and 2.

Unlike the above two topologies, topology $\mathbf{W}_{\mathrm{Random}} \in \mathbb{R}^{N\times N}$ is not constrained by the direction of node coupling, allowing for the random coupling of arbitrary spatial nodes:

$$\mathbf{W}_{\mathrm{Random}} = \begin{cases} \mathrm{rand}(N),\ \text{with probability } D \\ 0,\ \text{with probability } 1-D, \end{cases} \tag{5}$$

$D \in [0,1]$ represents the matrix node connection density. The topology structures vary with the density for the $\mathbf{W}_{\mathrm{Random}}$ topology is presented in Supplementary Figure 3.

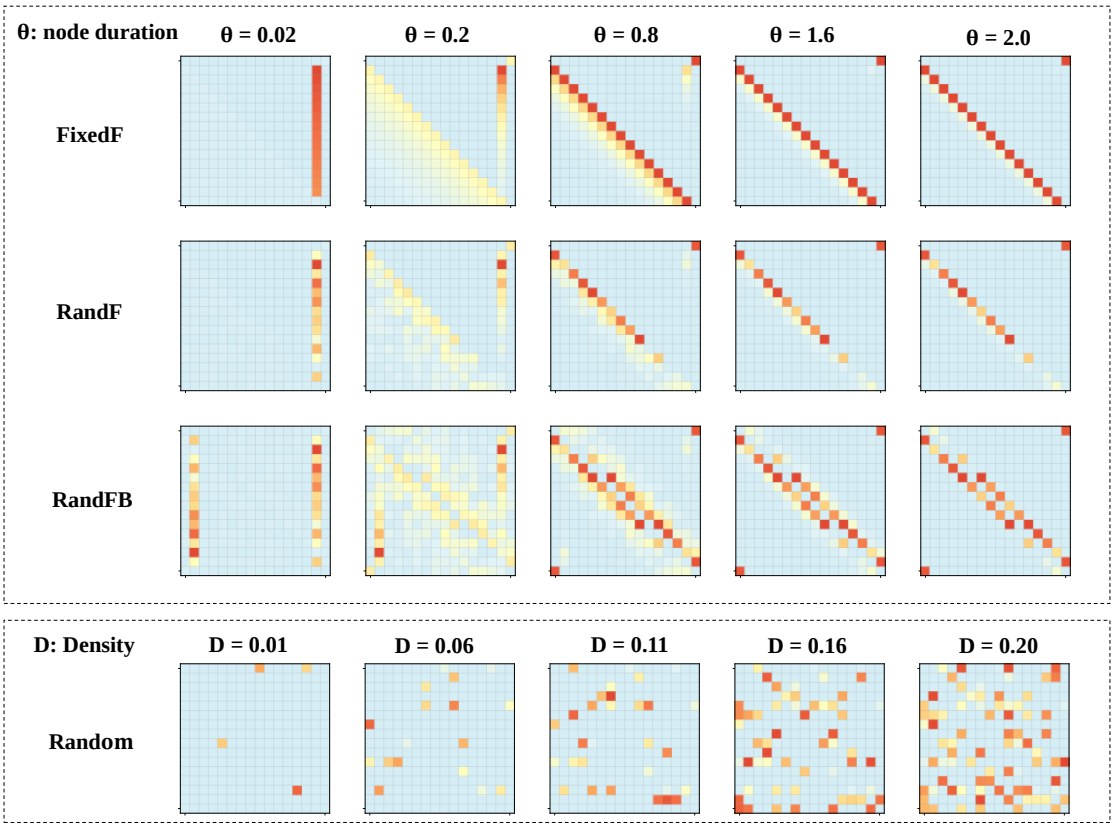

Supplementary Figure 1. Topology structure changes with variations in connectivity density. The topology structures with diagonal interconnection matrices of FixedF, RandF, and RandFB change with variations in node duration θ at values of 0.02, 0.2, 0.8, 1.6, and 2.0, which are systematically scanned. Meanwhile, the topology structure with Random matrices changes with variations in density D from 0.01 to 0.20.

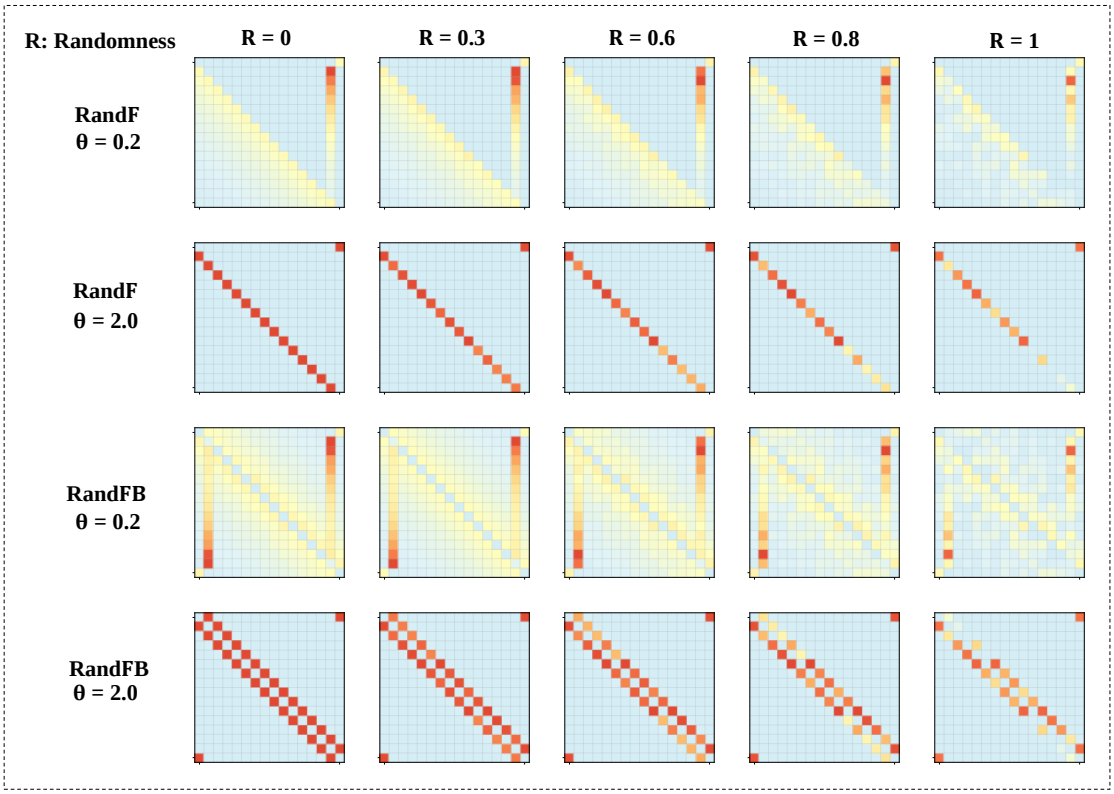

Supplementary Figure 2. Topology structure changes with variations in Randomness. The topology structures vary with the magnitude of randomness from 0 to 1 for both types of direction-related topology structures RandF and RandFB under fixed node duration θ=0.2 and 2.0.

Supplementary Note 2: Effects of topological structure randomness on MFI identification accuracy

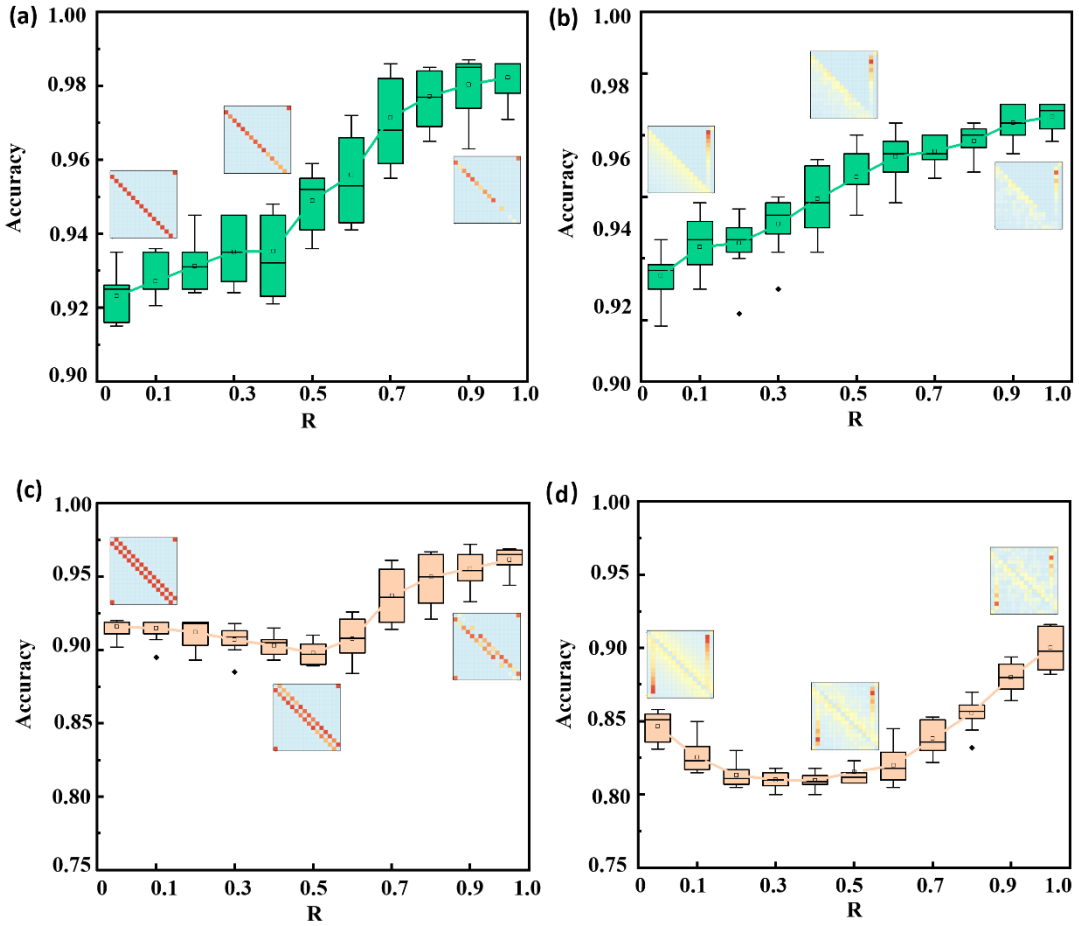

Supplementary Figure 3. Relationship between MFI recognition accuracy and the magnitude of randomness R introduced in the topology structures with fixed node duration θ. (a) θ = 0.2 for RandF (b) θ = 2.0 for RandF and (c) θ = 0.2 for RandFB (d) θ = 2.0 for RandFB.

Supplementary Fig. 3 provides a detailed relationship between MFI recognition accuracy and the magnitude of randomness introduced in the topology structures when the node duration θ is fixed at 0.2 and 2.0 for RandF and RandFB. The results indicate that the topology connections achieve the highest recognition accuracy when the introduced randomness R is strongest, and their performance is significantly superior to fixed topological connections without randomness.

Supplementary Note 3: System reconfigurability to adapt to varying channel bandwidths

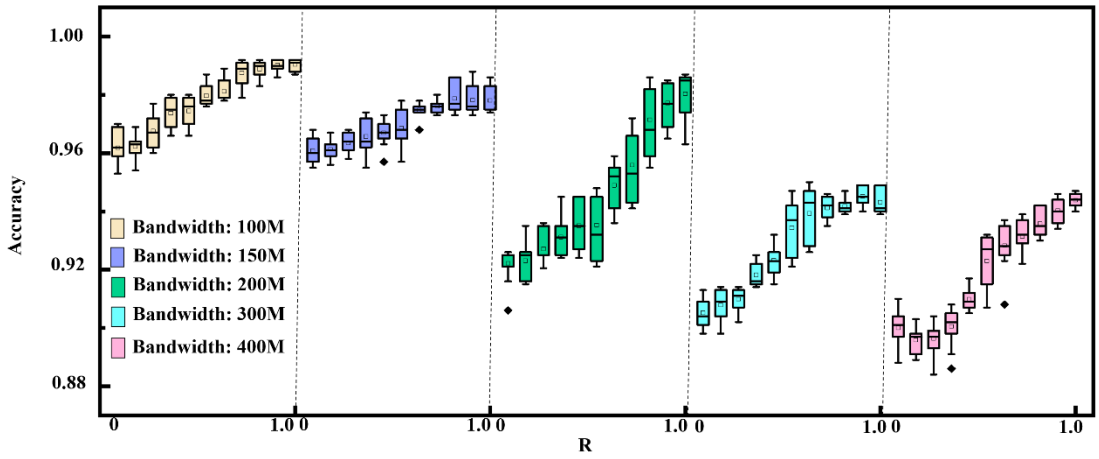

Supplementary Figure 4. The recognition accuracy of modulation format under different optical channel bandwidths varies with the level of randomness in the RC topology RnadF.

Achieving high-accuracy MFI is challenging due to bandwidth limitations and variable optical communication channels. Our RC system remains effective with retraining when the bandwidth varies from 100MHz to 400MHz. In particular, when the optical communication system's channel bandwidth is between 100 and 200MHz, the RC system can achieve modulation format recognition accuracy exceeding 98%. Despite the overall trend of decreasing recognition accuracy with increasing bandwidth, the flexibility in the RC system's topology allows for robust performance even in challenging conditions. Specifically, when the system bandwidth reaches 400MHz, the recognition accuracy can still reach 93% when the RC topology randomness (R) is at its maximum of 1.

Supplementary Note 4: Reconfigurable RC computing architecture is demonstrated in a benchmark task of nonlinear channel equalization

This benchmark task of nonlinear channel equalization was initially introduced in Ref [2] and first used in the realm of RC in Ref [3]. The objective is to retrieve an input symbol sequence $d(n)$ from the signal captured at the output $u(n)$, of a standardized nonlinear multipath RF channel, which is defined as follows:

$$\begin{aligned} q(n) = {} & 0.08d(n+2) - 0.12d(n+1) + d(n) \pm 0.18d(n-1) \\ & -0.1d(n-2) + 0.091d(n-3) - 0.05d(n-4) \\ & +0.04d(n-5) + 0.03d(n-6) + 0.01d(n-7) \end{aligned} \quad (6)$$

$$u(n) = q(n) + 0.036q^2(n) - 0.011q^3(n) + v(n) \quad (7)$$

The symbols $d(n)$ is randomly selected from a set of four values $\{3, -3,\ 1, -1\}$. In this context, $v(n)$ represents Gaussian noise with a mean of zero, calibrated to achieve Signal-to-Noise Ratios (SNRs) spanning from 12 to 32 dB. The assessment of performance is conducted based on the symbol error rate (SER), quantifying the proportion of incorrectly classified symbols.

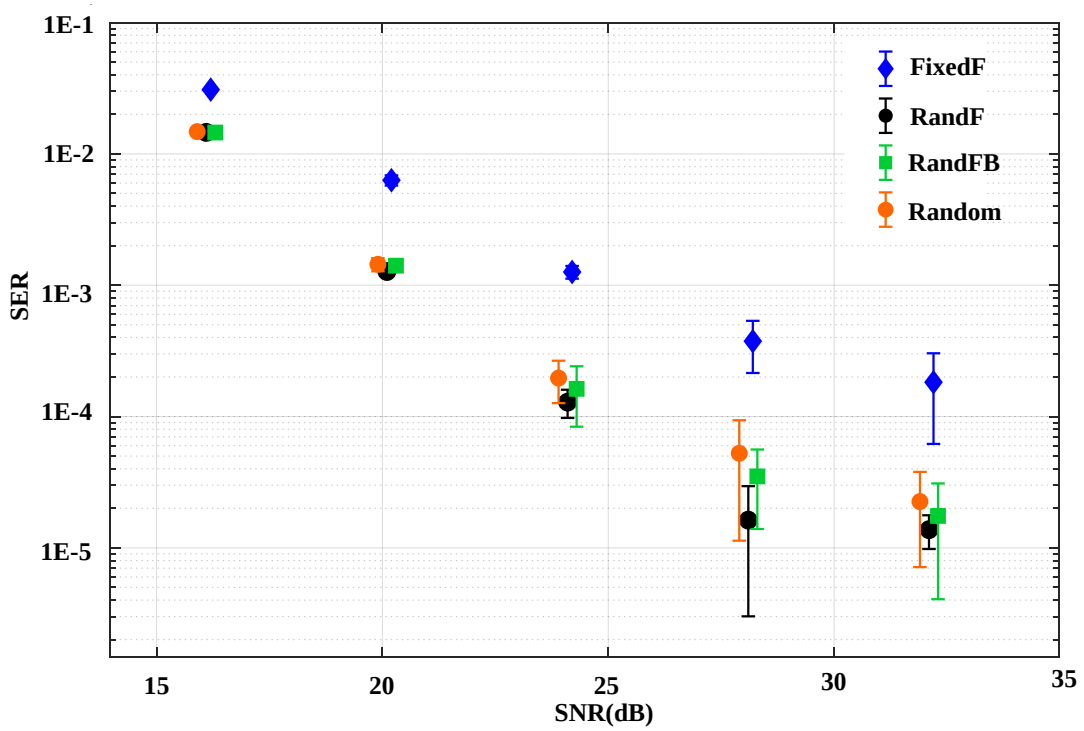

Supplementary Figure 5. SER vs SNR of reconfigurable RC of different topology. Results for nonlinear channel equalization task under reconfigurable topology. The horizontal axis is the SNR of the channel. The vertical axis is the SER, that is the fraction of input symbols that are misclassified.

As illustrated in Supplementary Figure 5, its evident that for SNRs ranging from 12 to 32 dB, reconfigurable topologies achieved lower SER in equalizing channel nonlinearity, outperforming the fixed baseline FixedF architectures. These results highlight the advantages of the reconfigurable method and confirm the high plasticity and adaptability of constructing high-performance RC systems for diverse applications.

Methods	Modulation formats number	Feature Extraction	Accuracy
DSP[4]	4	PAPR[a]	96%
MLP3-ANN[5]	6	AAHs[b]	99%
OEO-RC[6]	11	None	89%
Laser-P-RC[7]	3	AAHs	95%
MLP3-ANN[8]	10	PCA[c]	98%
CTA-RC[9]	6	CTAF[d]	90%
CIKD-NN[10]	8	CIKD[e]	87%
OEO/ISPP-RC[11]	16	AAHs / None	99.5 / 97.6%
Reconfigurable -RC	**6**	**AAHs**	**99.8%**

[a]Peak-to-average-power ratio. [b]Asynchronous amplitude histograms. [c]Principal component analysis. [d]Coordinate transformation and folding algorithm. [e]communication-informed knowledge distillation

Supplementary Table 1. Identification accuracies for different modulation formats using various systems.

Supplementary Note 5: Hardware platform of the system

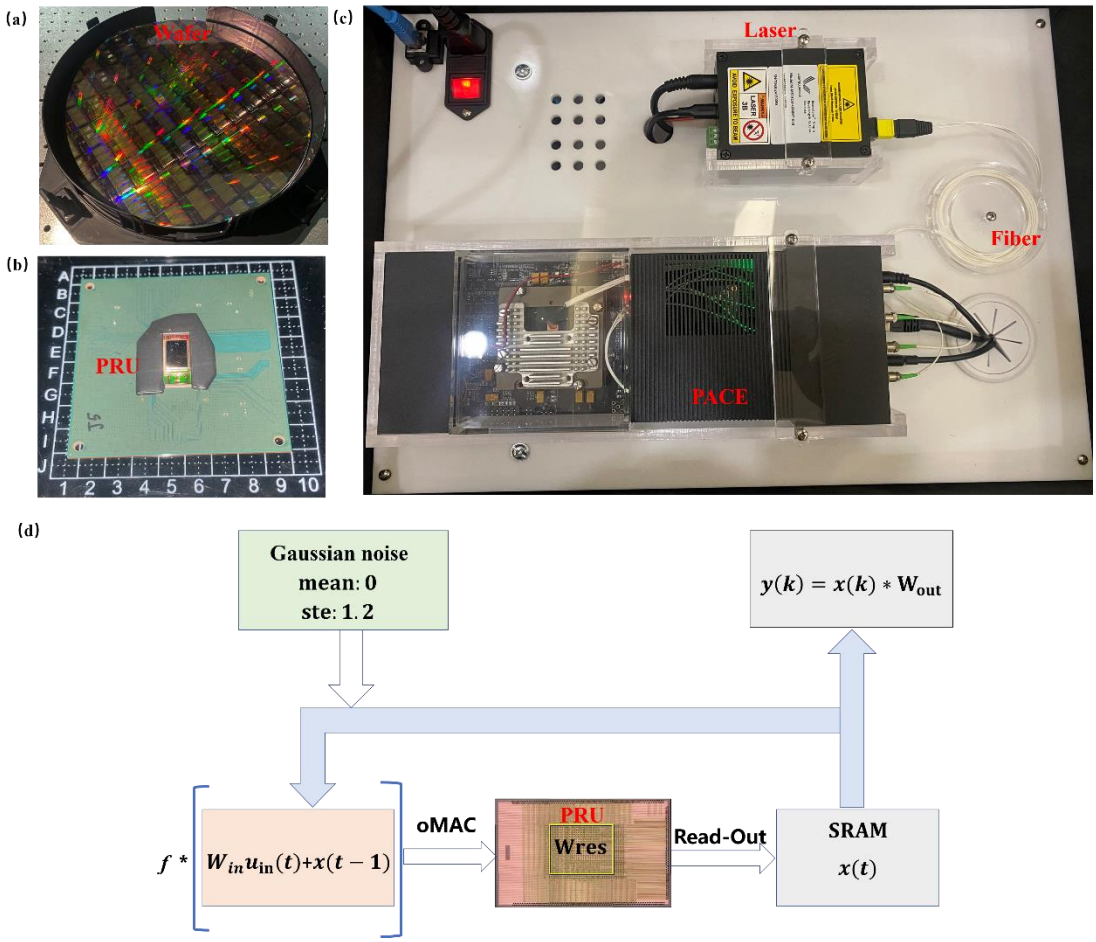

Supplementary Figure 6. Hardware platform of the system. (a) Optical core fabricated on a 12-inch SOI wafer using CMOS-compatible processes. (b) Photonic reservoir unit. (c) Integrated PACE system. (d) Pipeline of optoelectronic control for recurrent reservoir computing

The photonic reservoir unit (PRU) is realized on a silicon photonic processor featuring a 64 × 64 MZI mesh. The photonic chip and its electronic control circuits are co-packaged into the PACE module by Lightelligence Pte. Ltd[12]. Fabricated on a 12-inch SOI wafer using CMOS-compatible processes (Figure. 6(a)), The MZI mesh supports both arbitrary unitary and real-valued matrix operations. To realize high-density signal interconnects, the PACE system employs a 2.5D advanced-packaging solution—using flip-chip bonding to integrate the PIC, EIC, and substrate—as shown in Figure 6(b). Input data are optically modulated and coupled via fiber arrays, (Figure. 5(c)), and output signals are detected by high-speed photodetectors. At a modulation rate of 1 GHz, the processor achieves a matrix–vector multiplication rate of 8.19 TOPS. Figure. 5(d) shows the pipeline of optoelectronic control for recurrent reservoir computing.

Supplementary references

1. Paquot, Y., et al. Optoelectronic reservoir computing. *Sci Rep* **2**, 287 (2012).
2. Mathews, V. J. & Lee, J. Adaptive algorithms for bilinear filtering. In: *Advanced Signal Processing: Algorithms, Architectures, and Implementations V*). SPIE (1994).
3. Jaeger, H. & Haas, H. Harnessing nonlinearity: predicting chaotic systems and saving energy in wireless communication. *Science* **304**, 78-80 (2004).
4. Muhammad, S., et al. Blind modulation format identification for digital coherent receivers. *Opt Express* **23**, 26769-26778 (2015).
5. Guesmi, L., Ragheb, A. M., Fathallah, H. & Menif, M. Experimental Demonstration of Simultaneous Modulation Format/Symbol Rate Identification and Optical Performance Monitoring for Coherent Optical Systems. *Journal of Lightwave Technology* **36**, 1-1 (2018).
6. Dai, H. & Chembo, Y. K. Classification of IQ-Modulated Signals Based on Reservoir Computing With Narrowband Optoelectronic Oscillators. *IEEE Journal of Quantum Electronics* **57**, 1-1 (2021).
7. Cai, Q., et al. Modulation format identification in fiber communications using single dynamical node-based photonic reservoir computing. *Photonics Research* **9**, (2021).
8. Ali, A. K., Erelebi, E. & Engineering. Modulation Format Identification Using Supervised Learning and High-Dimensional Features. *Arabian Journal for Science Engineering* **48**, 1461-1486 (2022).
9. Li, F., et al. Modulation format recognition in a UVLC system based on reservoir computing with coordinate transformation and folding algorithm. *Opt Express* **31**, 17331-17344 (2023).
10. Yao, L., et al. Modulation format recognition in a UVLC system based on an ultra-lightweight model with communication-informed knowledge distillation. *Opt Express* **32**, 13095-13110 (2024).
11. Tang, D., Liang, E., Zhao, H. & Li, Z. All-optical implementation of an optoelectronic oscillator reservoir computer with an integrated spatial photonic processor. *Opt Lett* **50**, 2338-2341 (2025).